

# Discussion on data correction for Polarization Analysis with a $^3\text{He}$ spin filter analyzer

Earl Babcock<sup>\*1</sup>, Zahir Salhi<sup>1</sup>, Emmanuel Kentzinger<sup>2</sup>, Stefan Mattauch<sup>1</sup>, Alexander Ioffe<sup>1</sup>

<sup>1</sup>Jülich Centre for Neutron Science (JCNS) at Heinz Maier-Leibnitz Zentrum (MLZ), Forschungszentrum Jülich GmbH 85747 Garching, Germany,

<sup>2</sup> Jülich Centre for Neutron Science JCNS and Peter Grünberg Institut PGI, JARA-FIT Forschungszentrum Jülich GmbH, 52425 Jülich, Germany

E-mail: \* e.babcock@fz-juelich.de

**Abstract.** Fully polarized neutron reflectometry and grazing incidence small angle neutron scattering are effective methods to explore magnetic structures on the nm to  $\mu\text{m}$  length scales. This paper is an outline of how to fully correct for the polarization analysis (PA) inefficiencies of such an instrument and to determine the error contributions of the neutron polarizer and analyzer. This discussion considers the exact case of the polarization analysis instrumentation used on the MARIA neutron reflectometer at the MLZ or for a general polarized neutron scattering instrument using at least one  $^3\text{He}$  neutron spin filter that has the capability for adiabatic fast passage nuclear magnetic resonance flipping of the  $^3\text{He}$  polarization. This paper will work to build a conceptual understanding of how the inefficiencies of neutron polarization elements affect measured data in order to stress and encourage the application of PA corrections and to help perform successful measurements. Then, using data from a fully polarized neutron reflectometer test measurement we show how it is possible to recover signals on the order of, or even smaller than, the inefficiencies, or bleed-through, of the neutron polarization devices used.

## 1. Introduction

Neutron reflectometry and grazing incidence small angle neutron scattering (GISANS) with polarization analysis allow depth-resolved investigation of the magnetic structures in thin films and mesoscopic structures deposited on a surface. Neutron reflectometry gives access to in-plane averaged information and GISANS to correlations between in-plane variations, if those correlations appear on length scales smaller than the projection of the coherence volume of the beam on the sample surface. In the non-spin-flip (NSF) channels, one has access to the nuclear correlations and to the component of the fields parallel to the beam polarization vector and, in the spin-flip (SF) channels, one has access to the component of the field perpendicular to it. Therefore, by comparing the SF and NSF channels, one obtains vector information on the magnetic fields and their lateral correlations. Such studies are possible on the JCNS magnetism neutron reflectometer, MARIA [1] which uses a  $^3\text{He}$  spin filter as the analyzer element.

In this paper we will follow the formalism presented by A. Wildes [2, 3] where the matrix method was used to describe the polarization ( $P$ ), analysis ( $A$ ), and flipper ( $+F$ ) efficiency correction problem in polarized neutron scattering. Such corrections are implemented in software



for polarized instruments at the Institute Laue Langevin and NIST for example but here we look at how such corrections affect measured data to obtain a conceptual understanding also discussing the error sources and propagation. Finally the discussion can be applied to analysis of data from our MARIA reflectometer [1] which is used as an example.

A typical neutron scattering instrument would have a polarizer,  $P$  followed by a polarization flipper  $F$  before the sample, then another flipper after the sample followed by a polarization analyzer  $A$ . This document will solve the equations for two sub-cases of those described in [2, 3], one where the neutron flippers have ideal efficiencies, and two where one flipper is of a known and arbitrary efficiency, but the other flipping efficiency is perfect. The first case is to aide the conceptual understanding and stress the importance of PA corrections, and the second is the actual case for our MARIA reflectometer [1] where the polarization analyzer utilizes adiabatic fast passage reversal of the  $^3\text{He}$  nuclear polarization [4, 5, 6, 7] which makes  $A$  reversible negating the need for the second flipper. For this instance all the parameters of the  $PA$  and flipper ( $+F$ ) efficiencies can be explicitly determined with neutron transmission measurements (see Appendix B for details), thus allowing full correction of the measured cross-sections up to statistical and systematic error levels. The resulting discussion can be used as a recipe for  $PAF$  data corrections on instruments such as MARIA, including those with possible  $^3\text{He}$  polarization time-dependence.

In a full  $PA$  experiment, one would measure four scattering intensities,  $I^{00}$ ,  $I^{01}$ ,  $I^{10}$  and  $I^{11}$ , corresponding to the four possible combinations of the polarizer and analyser spin state. These intensities are then related to the two spin flip ( $\Sigma^{+-}$  and  $\Sigma^{-+}$ ) and two non-spin flip ( $\Sigma^{++}$  and  $\Sigma^{--}$ ) cross-sections with the relations derived in this work. From these four cross-sections the proportions of nuclear, magnetic and incoherent scattering can be obtained which can be applied for data from arbitrary scattering/detector geometries [8]. The main purpose of this discussion is both to guide in the practical data procurement and treatment in  $PA$  experiments, as well as to aide in a conceptual understanding of the relation between measured intensity data and the limits to the observable cross-section information contained within.

Beginning with the first case we derive the expressions for ideal neutron flipper inefficiencies as this greatly shortens the expressions. Even though not the practical case, the resulting expressions help one to understand how the often more intense non-spin flip cross-sections are being mixed with the much less intense spin-flip cross-sections in the measured intensities. This can be particularly useful to help understand the view on the live display during a measurement, thus giving an idea of when an observed spin-flip signal contains information on the sample cross-sections vs. simply being polarization leakage or “bleed through” of the bright non-spin flip states onto the spin flip states because of the  $PA$  inefficiencies. The resulting understanding can then be useful for intuitively performing effective neutron measurements. However as will be shown using a sample data set (see fig. 4), for an instrument such as MARIA even a low incident beam flipper inefficiency can lead to a spurious asymmetry in measured spin-flip intensities because this flipper is active in only two of the total four measured intensities. Therefore to correct the actual data, the discussion will then be extended to include the incident beam flipper inefficiency as well.

Finally, data obtained from a test measurement will be  $PAF$  corrected using the before described relations. This data will show visually the effects and robustness of the  $PAF$  inefficiency corrections by displaying the measured intensity plots next to the corrected cross-section plots with the resulting error contributions given. From this data it will be clear that in cases where there is no spin-flip scattering cross-sections, such as for saturated magnetic layers, the measured intensities are to first order simply the bleed through from the relative intensities of the non-spin-flip states times the sum of the polarization inefficiencies. As a result the amplitudes will go to zero in the corrected cross-section data, giving us confidence in data that does contain spin-flip scattering cross-sections even if their amplitudes lie below the  $PAF$  inefficiencies once the data is appropriately corrected.

## 2. Derivation of the $PA$ correction equations

We use the polarization matrix method summarized by A. Wildes in [2] to derive the  $PA$  corrections. The full matrices for the neutron polarization after scattering are as follows;

$$\begin{aligned}
 \begin{bmatrix} I^{00} \\ I^{01} \\ I^{10} \\ I^{11} \end{bmatrix} &= \begin{bmatrix} (1-p_1) & 0 & p_1 & 0 \\ 0 & (1-p_1) & 0 & p_1 \\ p_1 & 0 & (1-p_1) & 0 \\ 0 & p_1 & 0 & (1-p_1) \end{bmatrix} \begin{bmatrix} (1-p_2) & p_2 & 0 & 0 \\ p_2 & (1-p_2) & 0 & 0 \\ 0 & 0 & (1-p_2) & p_2 \\ 0 & 0 & p_2 & (1-p_2) \end{bmatrix} \\
 &\times \begin{bmatrix} 1 & 0 & 0 & 0 \\ 0 & 1 & 0 & 0 \\ f_1 & 0 & (1-f_1) & 0 \\ 0 & f_1 & 0 & (1-f_1) \end{bmatrix} \begin{bmatrix} 1 & 0 & 0 & 0 \\ f_2 & (1-f_2) & 0 & 0 \\ 0 & 0 & 1 & 0 \\ 0 & 0 & f_2 & (1-f_2) \end{bmatrix} \begin{bmatrix} \Sigma^{++} \\ \Sigma^{+-} \\ \Sigma^{-+} \\ \Sigma^{--} \end{bmatrix} \quad (1)
 \end{aligned}$$

In the experiment one measures the normalized intensities  $I^{00}$ ,  $I^{01}$ ,  $I^{10}$ , and  $I^{11}$  which are the convolution of the instrument's  $PA$  parameters and the scattering from the sample whereas  $\Sigma^{++}$ ,  $\Sigma^{+-}$ ,  $\Sigma^{-+}$  and  $\Sigma^{--}$  are the physical scattering contributions, or cross-sections themselves. The indices on  $I$  refer to the digital on (1) or off (0) state of the neutron flippers, i.e. a setting in the measurement script, whereas the indices on  $\Sigma$  refer to the polarization, or spin, of the neutrons before or after the sample being aligned parallel (+) or anti-parallel (-) to the magnetic holding field. The above matrix gives a set of linear equations that can be solved in terms of the intensities for  $\Sigma^{xy}$  if the flipper inefficiencies,  $f_1$  for the incident beam,  $f_2$  for the scattered beam, and the polarizing inefficiency  $p_1 = (1-P)/2$  and the analyzer inefficiency  $p_2 = (1-A)/2$  are known. Here  $P$  and  $A$  are the neutron polarization powers of the polarizer and analyzer respectively. We first solve the above relation for the case of ideal flippers (inefficiency=0) and arbitrary  $p_1$  and  $p_2$ . Performing the algebra one obtains;

$$\Sigma^{++} = \frac{I^{00}(1 + p_1p_2 - p_1 - p_2) + I^{01}(p_1p_2 - p_2) + I^{10}(p_1p_2 - p_1) + I^{11}p_1p_2}{(1 - 2p_1)(1 - 2p_2)} \quad (2)$$

$$\Sigma^{+-} = \frac{I^{01}(1 + p_1p_2 - p_1 - p_2) + I^{00}(p_1p_2 - p_2) + I^{11}(p_1p_2 - p_1) + I^{10}p_1p_2}{(1 - 2p_1)(1 - 2p_2)} \quad (3)$$

$$\Sigma^{-+} = \frac{I^{10}(1 + p_1p_2 - p_1 - p_2) + I^{11}(p_1p_2 - p_2) + I^{00}(p_1p_2 - p_1) + I^{01}p_1p_2}{(1 - 2p_1)(1 - 2p_2)} \quad (4)$$

$$\Sigma^{--} = \frac{I^{11}(1 + p_1p_2 - p_1 - p_2) + I^{10}(p_1p_2 - p_2) + I^{01}(p_1p_2 - p_1) + I^{00}p_1p_2}{(1 - 2p_1)(1 - 2p_2)} \quad (5)$$

In these equations one can see the appearance of the incident polarization,  $P = (1 - 2p_1)$ , and the analyser efficiency  $A = (1 - 2p_2)$ , where the factor of two in these relations comes from the definition of a polarization ( $A$  and  $P$ ) vs. the definition of the polarization inefficiencies used in eq. (1) which are simply the fraction of spins oriented the “wrong” direction [9]. Thus the data are normalized to the total instrumental analyzing power, and the factors multiplied by each measured  $PA$  state show how the mixed spins of the neutron beam contaminates the measured data. For a conceptual understanding of the importance of these corrections, let us assume  $\Sigma^{++} \simeq \Sigma^{--}$ ,  $\Sigma^{+-} \simeq \Sigma^{-+}$  and that the analyzing power and polarizing power are matched, i.e.  $p_1 \simeq p_2$ . Note, cross-section information in the analyzed data for the spin flip states diverges to 0 for a measured asymmetry of  $I^{01}/I^{00} \simeq F_{SF} \simeq ((I^{11}/I^{00})p_1 + p_2)/(1 - p_1 - p_2)$  where

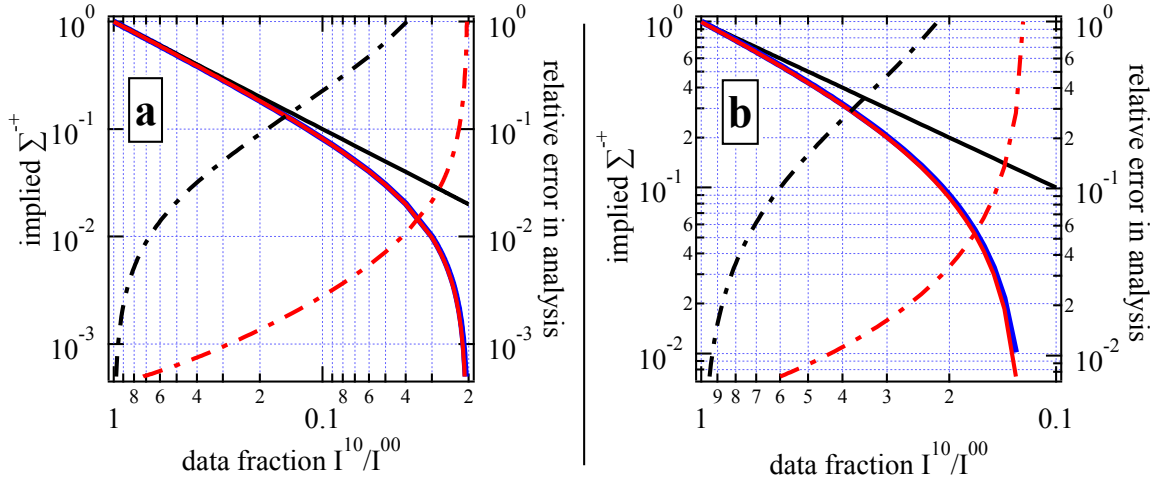


**Figure 1.** Influence of the the  $PA$  corrections on the observed signals for (a) balanced polarizer analyzer inefficiency of 98% or  $p_1 = p_2 = 0.01$  and (b) for imbalanced  $PA$  with analyzing inefficiency of 80% or  $p_2 = 0.1$  and a polarizer inefficiency of  $p_1 = 0.01$ . This shows that  $PA$  corrections become important for scattering at the level of the sum of the polarization inefficiencies. Left axis: the black line is the fraction of the measured signal  $I^{10}/I^{00}$ , the blue lines are the relative cross-section  $\Sigma^{-+}$  and the red line is the partially corrected signal where  $^*\Sigma^{-+} = I^{10} - I^{00}p_2 - I^{11}p_1$ . Right axis: the dot-dash lines are the respective relative error in assuming that the black (uncorrected intensities line) or red lines (first order corrected lines) represent the cross-section.

$F_{SF}$  is the relative apparent spin flip scattering fraction of a measured feature for a given  $(\alpha_i, \alpha_f)$  pair compared to the non-spin-flip scattering where  $\alpha_i$  is the neutron angle of incidence on the sample and  $\alpha_f$  is the final angle after reflection from the sample. For practical cases this implies the error diverges for  $I^{01}$  or  $I^{10} \leq p_1 + p_2$ . Thus, for example if  $p_1 = p_2 = 0.01$ , a rather acceptable 98% polarization and analyzing power, then the spin flip cross-section data in the  $I^{01}$  or  $I^{10}$  channels is invisible for  $I^{10} \simeq I^{01} \simeq 2\% \simeq p_1 + p_2$  if  $PA$  corrections are not made. As one can see in fig. 2 (a), for ratios of signal intensities of  $0.1 \simeq I^{10}/I^{00}$  the mixing of the wrong spin states already leads to high error. One may be inclined to do a first order correction ignoring the crossed terms containing the  $p_1p_2$  or  $p_x^2$  terms, however in fig. 2 (a) one can see that using the approximation  $^*\Sigma^{-+} \simeq I^{10} - I^{00}p_2 - I^{11}p_1$  still only allows recovery of signals on the order  $F_{SF} \simeq 2\%$  where the error diverges, and further this process actually over subtracts the spin mixing from the data. Fig. 2 (b) shows the same plots but for vastly imbalanced  $PA$  using a spin filter with  $p_2 = 0.1$  and a polarizer with  $p_1 = 0.01$  corresponding to a polarizer efficiency of 98% and an analyser efficiency of around 80%, nevertheless one arrives at the same conclusion. This shows conceptually that if one needs to observe spin flip signals overlapping strong non-spin-flip signals in Q space, i.e. occurring at the same  $(\alpha_i, \alpha_f)$ , the corrections become critical at the level of  $p_1 + p_2$  and therefore must be known to a good statistical accuracy. Conversely for intense spin-flip signals above this level, or for well resolved spin-flip and non-spin-flip signals in Q space, the first order correction when performed properly is readily sufficient to obtain up to 1% systematic accuracy in the processed data.

### 3. Full $PA$ correction equations with an imperfect incident beam flipper, $+F$

The equations provided up to this point help one understand how  $PA$  inefficiencies affect measured intensity data, but they are not sufficient to correct measured data from an instrument with a non-perfect  $f_1$  flipper inefficiency. Therefore solving eq. (1) assuming necessary corrections for  $p_1$ ,  $p_2$  and  $f_1$ , which is the actual case for MARIA, the above relations become;

$$\Sigma^{++} = \frac{I^{00}((1 + p_1 p_2 - p_1 - p_2)(1 - f_1) - f_1(p_1 p_2 - p_1))}{(1 - 2p_1)(1 - 2p_2)(1 - f_1)} \quad (6)$$

$$+ \frac{I^{01}((p_1 p_2 - p_2)(1 - f_1) - p_1 p_2 f_1) + I^{10}(p_1 p_2 - p_1) + I^{11} p_1 p_2}{(1 - 2p_1)(1 - 2p_2)(1 - f_1)}$$

$$\Sigma^{+-} = \frac{I^{01}((1 + p_1 p_2 - p_1 - p_2)(1 - f_1) - f_1(p_1 p_2 - p_1))}{(1 - 2p_1)(1 - 2p_2)(1 - f_1)} \quad (7)$$

$$+ \frac{I^{00}((p_1 p_2 - p_2)(1 - f_1) - p_1 p_2 f_1) + I^{11}(p_1 p_2 - p_1) + I^{10} p_1 p_2}{(1 - 2p_1)(1 - 2p_2)(1 - f_1)}$$

$$\Sigma^{-+} = \frac{I^{10}(1 + p_1 p_2 - p_1 - p_2)}{(1 - 2p_1)(1 - 2p_2)(1 - f_1)} \quad (8)$$

$$+ \frac{I^{11}(p_1 p_2 - p_2) + I^{00}((p_1 p_2 - p_1)(1 - f_1) - f_1(p_1 p_2 - p_1)) + I^{01}(p_1 p_2(1 - f_1) + p_2 f_1)}{(1 - 2p_1)(1 - 2p_2)(1 - f_1)}$$

$$\Sigma^{--} = \frac{I^{11}(1 + p_1 p_2 - p_1 - p_2)}{(1 - 2p_1)(1 - 2p_2)(1 - f_1)} \quad (9)$$

$$+ \frac{I^{10}(p_1 p_2 - p_2) + I^{01}((p_1 p_2 - p_1)(1 - f_1) - f_1(p_1 p_2 - p_1)) + I^{00}(p_1 p_2(1 - f_1) + p_2 f_1)}{(1 - 2p_1)(1 - 2p_2)(1 - f_1)}.$$

From analogy to the discussion where the flipper inefficiency was neglected, the result of this correction will again only become important when  $f_1 \simeq F_{SF}$ . Since a typical RF gradient flipper as used on MARIA can have an inefficiency on the order of  $1 \times 10^{-3}$  the corrections should be included to obtain a dynamic range beyond this level.

### 4. Examples from $PA$ corrections on polarized reflectometry data

We now apply the results of section 3 to correct the data from a test measurement of a  $\text{Fe}^{nat}\text{Fe}^{58}$  superlattice grating. The grating produced in KU Leuven and on loan from the ILL was a superlattice of 10 repeats of 10 nm layers of natural abundance Fe followed by 10 nm of isotopically enriched  $\text{Fe}^{58}$  that was sputtered on a 2 cm by 2 cm Si substrate. This superlattice was then etched with photo-resist methods to print a grating with a period of  $10 \mu\text{m}$  on it. This sample was then installed in the vertical sample magnet on MARIA where the detector arm scans the scattering in the horizontal plane with the grating lines also positioned vertically.

The MARIA instrument is a polarized neutron reflectometer with a horizontal-plane scattering geometry that uses a  $\Delta\lambda/\lambda = 10\%$  neutron velocity selector to choose the neutron wavelength [1]. The incident beam is polarized with a super-mirror and the incident beam flipper is a RF-gradient neutron flipper [6]. After the guide exit approximately 20 cm before the sample position, the neutron flight path was in air up to the position sensitive detector placed 200 cm after the sample position on the detector arm. For this experiment the analyzer was a 12 cm I.D.  $^3\text{He}$  neutron spin filter cell called “Idafix” [10] that is 8 cm long with 1.16 bar neutron calibrated  $^3\text{He}$  pressure and a 380 hour  $^3\text{He}$  lifetime in ideal laboratory conditions. The cell was polarized off-line and placed about 60 cm after the sample inside an 80 cm long permanent

magnet  $\mu$ -metal cavity producing a uniform magnetic field transverse to the neutron beam and sample magnet. This magnetic cavity had a rectangular solenoid RF-coil installed in it for the AFP flipping of the  $^3\text{He}$  [6, 7].

For this test the sample was installed in a vertical electromagnet capable of up to 1.1 T with the 5 cm gap pole shoes we used. The detector in this position gives us an angular resolution of around 0.3 mRad. For this measurement we chose to make  $\alpha_i$  steps of 0.9 mRad as a balance between resolution and the acquisition time required for reasonable statistics. Data was recorded for each  $\alpha_i$  line of an  $I^{\chi\psi}$  plot for 6 min, then the incident beam flipper was switched states to record the  $\alpha_i$  line for the other flipper state where the superscripts  $\chi$  and  $\phi$  refer to the state (i.e. 1 or 0) of the incident beam polarization and analyzer respectively. After a full  $\alpha_i$  scan for  $I^{00}$  and  $I^{10}$ , the  $^3\text{He}$  AFP flipper was used to reverse the  $^3\text{He}$  polarization and the detector arm was returned to the starting position and the  $\alpha_i$  scan is repeated for the  $I^{01}$  and  $I^{11}$  plots. For this particular test experiment the  $^3\text{He}$  spin filter was polarized offline in the JCNS spin-exchange optical pumping (SEOP) laboratory [11] and therefore had a time-dependent polarization. Since each pair of intensity plots took around 12 hours to acquire, the intensity data is corrected for the time dependent neutron transmittance of the  $^3\text{He}$  spin filter and the *PAF* corrections also use its time dependent  $A$  to solve for the corrected cross-sections.

Both the neutron analyzing power and transmittance of the  $^3\text{He}$  neutron spin filter cell are functions of the  $^3\text{He}$  polarization  $P_{He}$ , and neutron wavelength  $\lambda$  (see eqs. (14) and (15) in Appendix B) and can be explicitly calibrated with transmittance measurements. Then using the determined  $^3\text{He}$  cell parameters, the remaining  $P$  and  $F$  efficiencies can be obtained by measuring the instruments 2 flipping ratios  $\mathcal{F}^{\text{on}}$  and  $\mathcal{F}^{\text{off}}$  using the  $^3\text{He}$  APF flipper to reverse the analyzer polarization with the incident beam flipper on or off respectively. Further possible time changing  $^3\text{He}$  polarization, which normally follows an exponential decay, can be determined by repeating the transmittance calibration measurements periodically during the experiment. The result is all of the *PAF* efficiency parameters, and neutron transmittance can be explicitly characterized with simple calibration measurements on the direct neutron beam. A detailed description of the instrument calibration procedure used to perform the *PAF* corrections is given in Appendix B.

In order to correct the intensities to the time dependence, as follows from the full description in [3] the intensities  $I^{\chi\psi}$  are normalized to the neutron transmittance. As stated before reflectometry data using a fixed neutron wavelength is obtained by rotating  $\alpha_i$  stepwise recording one vertical  $\alpha_i$  line of an  $I^{\chi\psi}$  plot at a time. The measured intensities are thus transmittance normalized piecewise, using the deduced values for neutron transmittance  $T$  (from eq. 15 in Appendix B) for the actual time of the particular  $\alpha_i$  line in the recorded intensity (i.e.  $I^{\chi\psi}$ ) data. The resulting  $^3\text{He}$  cell transmittance and sample geometry corrected intensity data are lastly normalized to the total reflected intensity below the critical edge. The resulting transmittance corrected and normalized intensity plots are shown in figs. 2 (a) and 3 (a).

Now that the data has been  $^3\text{He}$  cell transmittance corrected over time and  $P$ ,  $A(t)$  and  $F$  have been calibrated, we apply the *PAF* corrections to the *PA* reflectometry measurement using the relations in section 3 to solve for the scattering cross-sections  $\Sigma^{xy}$ . As for the transmittance correction, we solve for the analyzing power  $A$  or equivalently  $p_2$  at the time of a particular  $\alpha_i$  line of an  $I^{\chi\psi}$  plot which are then used in eqs. (6-9) to create the *PAF* (and  $^3\text{He}$  time dependence) corrected cross-section plots. Thus there are different  $p_2$  from the different times for each  $\alpha_i$  line in the equations for a particular  $\Sigma^{xy}$ . This is because the polarization “beed-throughs” of each of the particular  $\alpha_i$  lines in the four  $I^{\chi\psi}$  plots need to be corrected for the inefficiencies at the time they were recorded in order to subtract/normalize the data the appropriate amount.

In the plots 2(a,b) and 3(a,b) we compare the corrected intensity data ( $I^{\chi\psi}$ ) from the reflectometry measurement on the left (a) to the corrected spin-flip cross-section data ( $\Sigma^{x,y}$ ) on the right (b). As stated before, the sample was an  $\text{Fe}^{\text{nat}}\text{Fe}^{58}$  superlattice (10 repetitions of



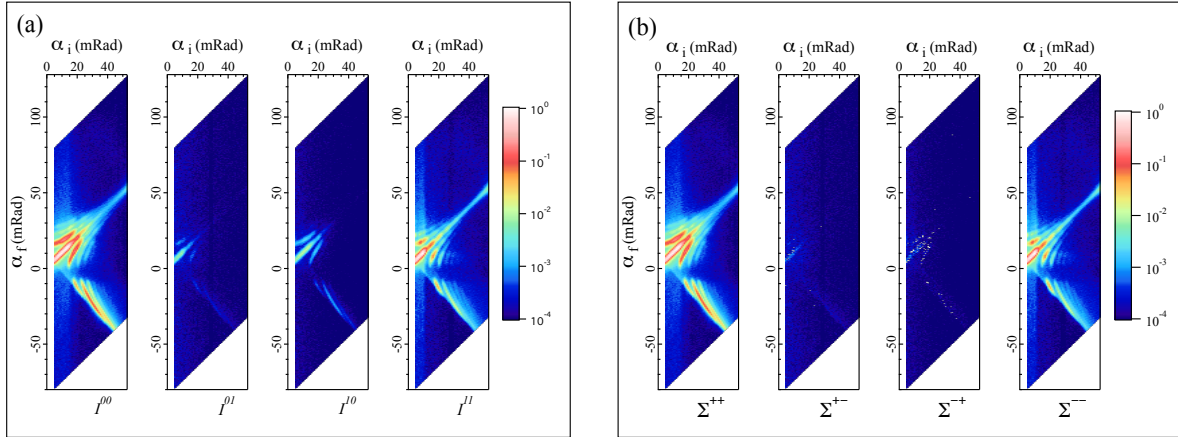


**Figure 2.** Polarized reflectivity and off-specular scattering data from the  $\text{Fe}^{\text{nat}}\text{Fe}^{58}$  superlattice grating sample with a 0.7 T saturation field applied. The grating lines of the sample aligned parallel to the applied field. In the intensity plot to the left (a) a small spin-flip like signal can be seen and it also contains an apparent asymmetry in the spin-flip channels, graphs  $I^{01}$  and  $I^{10}$ . However, when one performs the full *PAF* corrections in the plots of the scattering cross-sections on the right (b), these signals disappear. The fact that the *PAF* corrections become important when  $F_{\text{SF}} \simeq p_1 + p_2 + f_1$  is shown visually in this data as the sum of the inefficiency terms was  $\simeq 12 \times 10^{-3}$  for the  $I^{10}$  plot and  $\simeq 8 \times 10^{-3}$  for the  $I^{01}$  plot which are the approximate amplitudes of the data in these two intensity plots for data on the specular line below the critical edge. Close inspection of the specular scattering i.e.  $\alpha_i = \alpha_f$ , shows a dynamic range of about  $1 \times 10^{-4}$  is achieved in the polarized mode.

10 nm of each  $\text{Fe}^{\text{nat}}$  and  $\text{Fe}^{58}$ ) with a  $10 \mu\text{m}$  pitch grating etched on it. The plots 3 show the magnetically unsaturated sample with a remanent sample magnetization, and the plots 2 show the sample at a high field of 0.7 T where the magnetization should be fully aligned for the high field measurement, but not necessarily for the low field remanent measurement. In fig. 2 before the *PAF* corrections one can clearly see the leakage of the imperfect PA, but after corrections any possible spin-flip cross-sections are reduced to zero, or below the  $1 \times 10^{-4}$  which is the S/N floor of this particular measurement. Next, in fig. 3 we see how much of the apparent spin-flip signal in the uncorrected data on the left is removed in the corrected data on the right, however a certain amount of spin-flip scattering remains.

To show that this data is indeed significant we consider the error contributions resulting from the combination of four measured intensities in each corrected cross-section plot. We perform a simple error analysis by taking the partial derivatives of the eqs. (2-5) with some simplifications (see Appendix A) and in terms of relative errors we obtain the usual result:

$$(\delta\Sigma^{++})^2 \simeq (\delta I^{00})^2 + (I^{00}\delta p_1)^2 + (I^{00}\delta p_2)^2 + (I^{01}\delta p_2)^2 + (I^{10}\delta p_1)^2 \quad (10)$$

$$(\delta\Sigma^{+-})^2 \simeq (\delta I^{01})^2 + (I^{01}\delta p_1)^2 + (I^{01}\delta p_2)^2 + (I^{00}\delta p_2)^2 + (I^{11}\delta p_1)^2 \quad (11)$$

$$(\delta\Sigma^{-+})^2 \simeq (\delta I^{10})^2 + (I^{10}\delta p_1)^2 + (I^{10}\delta p_2)^2 + (I^{11}\delta p_2)^2 + (I^{00}\delta p_1)^2 \quad (12)$$

$$(\delta\Sigma^{--})^2 \simeq (\delta I^{11})^2 + (I^{11}\delta p_1)^2 + (I^{11}\delta p_2)^2 + (I^{10}\delta p_2)^2 + (I^{01}\delta p_1)^2. \quad (13)$$

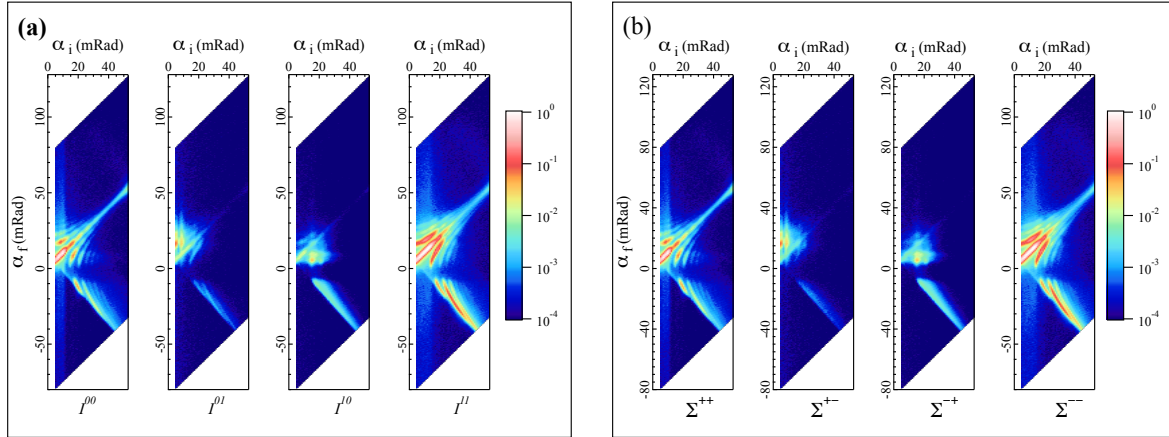


**Figure 3.** Polarized reflectivity and off-specular scattering data from the  $\text{Fe}^{\text{nat}}\text{Fe}^{58}$  superlattice grating sample with remanent magnetization. The sample was magnetized by momentarily applying a strong field of 0.7 T anti-parallel to the neutron guide field and then switching it to a nominal 10 G (1 mT), thus leaving an anti-parallel remanent magnetization in the Fe of the grating. The grating lines, as in the saturated state, are parallel to the applied guide field. (a) The intensities are shown to the left, and (b) the *PAF* corrected data to the right. In the *PAF* corrected data one sees there is indeed remaining spin-flip scattering that is not a result of the instrument *PAF* inefficiencies. The main qualitative difference between the corrected cross-section data and the intensities data is that upon close inspection, the corrected spin-flip cross-sections along the specular,  $\alpha_i = \alpha_f$ , line are reduced as are the apparent  $\pm 1$  order diffraction lines compared to the uncorrected data. The resulting spin-flip signals are thus coming from the sample with good confidence and are likely caused by a slight component of the in-plane magnetization in the sample being perpendicular to the applied field.

Here one can see how the subtraction of the more intense non-spin flip states from the weaker spin-flip ones will increase the resulting error bars of overlapping spin-flip data and since the flipper was a correction to the *P* and *A* corrections, it dropped out from the larger terms in the error budget. To show the effects visually, we used these formulas to calculate relative error bars for a the sample data set on the  $\text{Fe}^{\text{nat}}\text{Fe}^{58}$  grating given in figs. 2 and 3 assuming a 1% accuracy of the  $p_1$ ,  $p_2$  and  $f_1$  calibrations which are plotted in fig. 4 (a) and (b). The results indeed are acceptable as the error bars around features of interest where spin-flip scattering cross-sections are observed in fig. 4 (a) are clearly staying in the blue region which corresponds to 10% relative error or less for the data. Much of the remaining off-specular region are yellow corresponding to large ( $>0.5$ ) error because of the very low scattering and subsequent lack of signal in these areas. The black areas (relative error  $>1$ ) in fig. 4 (b) in the  $\Sigma^{+-}$  and  $\Sigma^{-+}$  around the specular line and where the diffraction pattern in the off-specular scattering was observed in the uncorrected data, as can be understood from eqs. 11 and 12 results from the subtraction of the much more intense  $I^{00}$  and  $I^{11}$  and its effect on the error budget, after subtraction of the more intense states the resulting corrected cross-sections in this area have amplitudes around the noise level of  $1 \times 10^{-4}$  but the error bars are equal to or slightly larger than this value. Finally a black vertical line of high error is visible at  $\alpha_i \simeq 30$  mRad in the  $\Sigma^{+-}$  and  $\Sigma^{-+}$  plots of 4 (b), this was likely caused by a temporary monitor or background instability, as due to the pairwise data acquisition these  $\alpha_i$  lines were taken in the same 30 min block of time during the 2 day long measurement. Consequently we can now make a qualitative assessment of how the data interpretation changes once the *PAF* corrections are applied. Features of such data has been nicely discussed in [15, 16, 20] for example. Here we describe them in terms of the DWBA



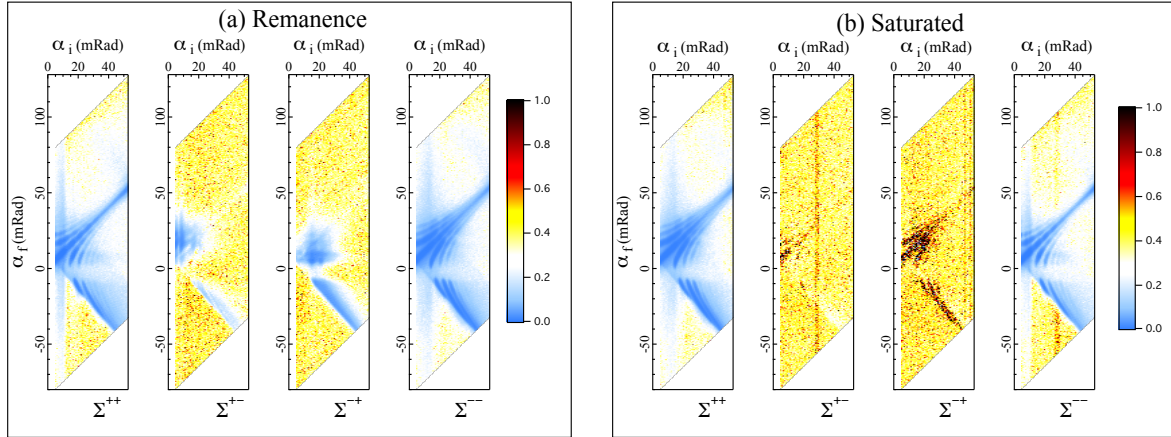


**Figure 4.** Plots of the relative error bars for *PAF* corrections for the remanent (a) and 0.7 T saturated (b) data calibrated to 1%. One can see in the areas of interest the relative error stays to approximately 10% or less, i.e the blue regions in the plots. In the (b) plots, the data around the specular line in the spin-flip channels has high relative error (black >100%) because the cross-section that the amplitude was essentially 0 to within the S/N after the *PAF* corrections.

formalism [17] as this is the basis for modelling and fitting software at the MLZ [18].

The data in fig. 2 (a) of the non *PAF* corrected images at 0.7 T sample field indeed show reflectivity and off-specular scattering intensity for the sample at magnetic saturation, further there is an asymmetry between  $I^{10}$  and  $I^{01}$ . However, once one performs the full *PAF* correction, it is apparent that the asymmetry comes from the incident beam flipper which is only “on” for the  $I^{10}$  and  $I^{11}$  scans, and the remaining apparent spin flip signal was simply the bleed-through of the polarizer and analyzer due to their inefficiencies. As clearly seen in the corrected data in fig. 2 (b), since all magnetizations lay parallel to the field, the spin-flip scattering from the sample vanishes to the accuracy of the measurement. Along the line  $\alpha_i = \alpha_f$  one obtains the specular reflectivity of the sample. Here, the critical angle of total reflection is bigger in the  $\Sigma^{++}$  channel than in the  $\Sigma^{--}$  channel because of the bigger average scattering length density. Away from this diagonal line, which is referred to as the off-specular scattering, the scattering wave vector has a component along the sample plane and up to three orders of Bragg scattering from the grating structure is observed. In the  $\Sigma^{++}$  channel, the scattering is on the average stronger than in the  $\Sigma^{--}$  channel. This can be explained if one considers the scattering amplitude in the framework of the distorted wave Born approximation (DWBA) [17]. In this formalism, the neutron-matter interaction potential is separated as a part obtained by in-plane averaging and a second part that describes the in-plane variations around this average. The first part leads to specular reflectivity and the second part to off-specular scattering. The scattering amplitude is no longer a Fourier transformation of the potential taken between the bra and ket that represent the wave function of the neutron after the sample (Born approximation), but a Fourier transform of the in-plane fluctuation potential taken between the bra and ket that represent the neutron wave function inside the laterally averaged potential. Those bras and kets are linear combinations of reflection and transmission amplitudes. As is evident from the specular intensities in the  $\Sigma^{++}$  and  $\Sigma^{--}$  channels, the reflection amplitudes for + neutrons are, on the average, more intense than in the – ones. This therefore explains why the off-specular scattering is more intense in the ++ channel and in the -- channel.

The fidelity of this high field 0.7 T data then gives us confidence in the data shown in fig. 3 (b). This figure shows the reflectivity and off-specular scattering from the sample at a field of 1 mT, after saturation in a strong antiparallel magnetic field. For this remanent magnetization scan

one can also see qualitative changes in the data. First, the intensity of the specular line in the spin-flip channels ( $\alpha_i = \alpha_f$ ) is noticeably reduced, next what had appeared as weak diffraction from the grating lines around the specular line turned out to be *PAF* inefficiency bleed through. The corrected data (fig. 3 (b)) show two main differences with respect to the ones at saturation (fig. 2 (b)). The first one is that the  $\Sigma^{++}$  intensities are now weaker than the  $\Sigma^{--}$  intensities, a result of the fact that all magnetizations are now aligned almost anti-parallel to the incoming beam polarization. The second one is the presence of reflectivity and off-specular signal in the spin flip channels  $\Sigma^{+-}$  and  $\Sigma^{-+}$ . This is a sign that the laterally averaged magnetizations are not exactly anti-parallel to the external field, but have a small component perpendicular to it. One can also see that the off-specular signal is not symmetric with respect to the diagonal  $\alpha_i = \alpha_f$ . This can be explained, once again, in the framework of the DWBA [17]. In the  $\Sigma^{+-}$  channel, the neutron beam before interaction with the sample is polarized up and after interaction with the sample the neutrons are selected with spin projection down. As the reflection amplitudes of + neutrons are, on the average, smaller than in the one of - neutrons, one observes smaller intensities of off-specular scattering in the  $\alpha_i > \alpha_f$  region than the ones in the  $\alpha_i < \alpha_f$  region. The same type of explanation holds for the intensities in the  $\Sigma^{-+}$  channel. However, if one were to sum the  $\Sigma^{+-}$  and  $\Sigma^{-+}$  the resulting image would exhibit mirror-plane symmetry about the specular line.

The data corrections in this case now allow us to qualitatively see spin-flip effects approaching the  $1 \times 10^{-4}$  level even though the sum of the *PAF* inefficiency terms was around  $1 \times 10^{-2}$ . This data has reasonable quantitative confidence as the total relative error bars including the statistical uncertainties and the additional error from the *PAF* corrections are on the order of 10% or better for the areas of interest. If the error in the *PAF* inefficiency calibrations was on the order of 10% rather than 1%, then the relative error bars in the spin flip signals observed in the remanent data would be around 15% for the region near the specular line. Conversely, the statistical error bar just from the neutron counting rates for the  $I^{01}$  and  $I^{10}$  intensities in this area were about 3% themselves. Thus with 1% *PAF* inefficiency calibration the total error was around 3 times higher than the statistical error of the uncorrected data for this example and would be about 5 times higher with a less precise 10% *PAF* inefficiency calibration.

## 5. conclusion and acknowledgements

When one has a saturated magnetic structure with no spin-flip scattering such as in fig. 2, the data itself can help refine or verify the *PAF* inefficiencies used for the corrected cross-section data. However this may not be the case for all real experiments on more complex systems so one should have confidence in the instrument calibration data and *PAF* inefficiency correction procedure to ensure when potential spin-flip scattering cross-sections obtained after *PAF* corrections are indeed significant. As was shown in the data presented in figs. 2 and 3 one can indeed correct even time-dependent neutron *PA* data, in this case taken with a time-decaying  $^3\text{He}$  spin filter if the *PAF* parameters can be calibrated to the appropriate level. For the data shown *PAF* corrected cross-sections were obtained to good confidence with a 1 to  $1 \times 10^{-4}$  dynamic range with statistically relevant error levels. Conversely the results of this paper should also make it clear the rule-of-thumb that non-*PAF* corrected polarized neutron data must be very carefully justified if the values of the relative cross-sections are on the order of the instrument's *PAF* inefficiencies unless such features are well separated from any intense non-spin-flip scattering features.

This paper explains the observed signal to noise including a discussion of error propagation and can serve as a recipe for data corrections in modern polarized neutron experiments, especially those employing a  $^3\text{He}$  spin filter cell as the analyzer, and is meant to encourage a conceptual understanding of *PAF* corrections and their application to aid good measurement strategy and in analyzing and publishing data. MLZ is developing software for modelling and fitting

layered structures with lateral correlations including the nuclear and magnetic structures using the DBWA [18]. We will work towards applying this software to the model multi-layered and patterned system data presented here, and presenting a discussion in future work.

We kindly acknowledge A. Wildes of the Institut Laue Langevin who provided the  $\text{Fe}^{\text{nat}}\text{Fe}^{58}$  patterned multilayer sample and K. Temst whose group in KU-Leuven produced it.

### Appendix A: error bar calculation for $PAF$ corrected cross-sections

In this appendix we summarize the error analysis which was used to calculate the error bars shown in figs.4. A polarized  $^3\text{He}$  neutron spin filter and be fully calibrated (see following Appendix B) to nearly arbitrary accuracy, consequently is it useful to show an error analysis in order to understand how the statistical accuracy of the measurement, vs. the precision of the instrument calibration contributes to the error of the corrected neutron PA cross-section data. Using the first spin-flip cross-section  $\Sigma^{+-}$  (eq. (8)) as an example and performing a simple error analysis of the full formula by taking the partial derivatives one obtains:

$$\begin{aligned}
 (\delta\Sigma^{+-})^2 = & \left( \frac{\delta I^{01}((1+p_1p_2-p_1-p_2)(1-f_1)-f_1(p_1p_2-p_1))}{PAF'} \right)^2 + \left( \frac{\delta p_1 I^{01}(1-p_2)}{P^2AF'} \right)^2 + \left( \frac{\delta p_2 I^{01}(2f_1p_1-f_1-p_1+1)}{PA^2F'} \right)^2 \\
 & + \left( \frac{\delta f_1 I^{01}(p_1-p_2p_1)}{PAF'^2} \right)^2 \\
 & + \left( \frac{\delta I^{00}((p_1p_2-p_2)(1-f_1)-p_1p_2f_1)}{PAF'} \right)^2 + \left( \frac{\delta p_1 I^{00}(-p_2)}{P^2AF'} \right)^2 + \left( \frac{\delta p_2 I^{00}(-2f_1p_1+f_1+p_1-1)}{PA^2F'} \right)^2 + \left( \frac{\delta f_1 I^{00}(-p_1p_2)}{PAF'^2} \right)^2 \\
 & + \left( \frac{\delta I^{11}(p_1p_2-p_1)}{PAF'} \right)^2 + \left( \frac{\delta p_1 I^{11}(p_2-1)}{P^2AF'} \right)^2 + \left( \frac{\delta p_2 I^{11}(-p_1)}{PA^2F'} \right)^2 + \left( \frac{\delta f_1 I^{11}(p_1p_2-p_1)}{PAF'^2} \right)^2 \\
 & + \left( \frac{\delta I^{10}(p_1p_2)}{PAF'} \right)^2 + \left( \frac{\delta p_1 I^{10}(-p_2)}{P^2AF'} \right)^2 + \left( \frac{\delta p_2 I^{10}(-p_1)}{PA^2F'} \right)^2 + \left( \frac{\delta f_1 I^{10}(-p_1p_2)}{PAF'^2} \right)^2
 \end{aligned}$$

for the relative error contribution  $\delta\Sigma^{+-}$  of the  $\Sigma^{+-}$  cross-section.  $P$  and  $A$  are again the polarization and analyzer efficiencies related to the inefficiencies by  $P = 1 - 2p_1$  and  $A = 1 - 2p_2$  and the flipper efficiency is momentarily defined as  $F' = 1 - f_1$  to simplify the written expressions. The other terms for the  $\Sigma^{+-}$ ,  $\Sigma^{-+}$ , and  $\Sigma^{--}$  can be obtained similarly. Using this eq. (14) to help us understand the dominate terms in the resulting error calculation, we discard all higher order terms containing products of  $p_1$ ,  $p_2$  and  $f_1$  terms which will be small. Now we see that the flipper errors don't contribute to the eventual error bars in the first order approximation and by further inspection for a system with low polarization element inefficiencies  $p_1$ ,  $p_2$ , and  $f_1$  we can set the denominators to 1. This gives us the result of the compact set of eqs. (10-13) given previously in section 4 to estimate the error contributions.

### Appendix B: instrument $PAF$ efficiency calibration

One of the very powerful features of using a polarized  $^3\text{He}$  spin filter with AFP spin flipping of the  $^3\text{He}$  polarization employed, is the ability to fully characterize the neutron polarization parameters under the exact instrument configuration and conditions of the scattering experiment. Although the  $P^2T$  quality factor of a  $^3\text{He}$  type analyzer may be lower than a large area super mirror array [19], their very deterministic nature which allows for simple calibration over all neutron wavelengths, their uniform and smooth analyzing power over large areas, and their ability to provide an arbitrarily high analyzing efficiency can outweigh the downsides of lower transmittance, required maintenance and possible time dependence for some instances. This method also avoids the complications of other neutron PA methods using two imperfect neutron flippers which require more involved instrument calibrations, a summary of which are included in the work of Williams [20] and also discussed in [3].

To quantify the *PAF* parameters we follow a method similar to that outlined in [21] where one simply measures the unpolarized neutron transmittance as a function of wavelength for the unpolarized and the polarized  $^3\text{He}$  cell. In [21] Chupp et. al. used a “white” neutron beam and time of flight where used to determine the neutron wavelength but on many instruments such as MARIA where PA is installed, white-beam time of flight is not available to calibrate the  $^3\text{He}$  spin filter cell. However MARIA [1] has a velocity selector that allows us to scan the neutron wavelength and determine discrete transmittance values and fit them as a function of neutron wavelength. The neutron analyzing (polarizing) power  $A(\lambda)$  and transmittance  $T(\lambda)$  of a  $^3\text{He}$  cell are can be derived from the neutron polarization dependent  $1/v$  cross-sections as in [22]. For a  $^3\text{He}$  spin filter the neutron analyzing power  $A(\lambda)$  and unpolarized neutron transmittance  $T(\lambda)$  as functions of the neutron wavelength  $\lambda$  are

$$A(\lambda) = \tanh(P_{He}\Theta\lambda\sigma), \quad (14)$$

$$T(\lambda) = T_0 \exp(-\Theta\lambda\sigma) \cosh(P_{He}\Theta\lambda\sigma) \quad (15)$$

where  $T_0$  is the empty cell transmittance,  $\sigma = 0.0732 \text{ bar}^{-1} \text{ cm}^{-1} \text{ \AA}^{-1}$  is polarization dependent neutron absorption cross-section of  $^3\text{He}$ , the  $^3\text{He}$  polarization is  $P_{He}$  and  $\Theta$  is the product of the spin filter cell's length in cm and  $^3\text{He}$  pressure in bar at 25 °C. For the reblown GE180 cells used in the MARIA SEOP analyzer we have tested many cells and found them to have a relatively uniform 88% to 91% transmittance for  $5 \text{ \AA} < \lambda < 10 \text{ \AA}$  which is similar to that found by others [21]. Therefore when we fit the unpolarized cell data, we leave  $T_0$  as wavelength dependent constant. Of course for highest accuracy one can also perform empty cell measurements to determine  $T_0$  which would have to be characterized before preparation for SEOP cells which are permanently sealed after being filled with  $^3\text{He}$  [23, 10], MEOP cells which are valved can be evacuated and essentially can be calibrated at any time [24]. Further in cases where the  $^3\text{He}$  spin filter cell has single crystal silicon neutron windows [25]  $T_0$  can be calculated from the Si neutron absorption cross-section and thickness.

To characterize the SEOP cells used on MARIA we measure the unpolarized neutron transmittance vs. wavelength typically with 4 to 5 steps from 5 Å to 10 Å for the cell when it is polarized, and completely depolarized. The polarized  $^3\text{He}$  analyser on MARIA is installed on a translation stage so the transmittance measurements are performed comparing the cell in beam to the cell out of beam intensity measurements. Unpolarized cell transmittance data is fit to eq. (15) with  $P_{He}$  set to 0 (i.e. fit to an exponential) to determine the value of  $\Theta$ . Then using this value of  $\Theta$  the polarized cell data can be fit to eq. (15) to determine  $P_{He}$ . One can also simply take the ratio of the cell transmission when the  $^3\text{He}$  polarized to its transmission with  $P_{He} = 0$  and perform a  $\cosh(P_{He}\Theta\lambda\sigma)$  fit to determine the product of  $P_{He}$  and  $\Theta$ . Since SEOP polarized  $^3\text{He}$  cells are permanently sealed, the unpolarized cell measurement to determine  $\Theta$  must not be repeated but occasionally for routine checks, and strictly speaking if  $\Theta$  and  $T_0$  of a particular cell are sufficiently characterized only one neutron wavelength is required to determine  $P_{He}$ . Using  $P_{He}$  and  $\Theta$  in eqs. (14) and (15) the analyzer's polarization efficiency and transmittance can be calculated for any neutron wavelength. For the cell used in the MARIA analyzer in this experiment, fits to unpolarized transmittance of the unpolarized cell over neutron wavelength gave us a value of  $T_0 = 0.89$  and  $\Theta = 9.27 \text{ bar cm}$ . The length  $l$  of this particular cell was about 8 cm, giving a cell pressure of 1.16 bar, however it is not required to know these numbers individually. Using the obtained  $\Theta$ , the  $^3\text{He}$  polarization from the cosh fit gave a starting value of  $P_{He} = 71.5\%$  for the experiment described in this paper. The exponential fit of the unpolarized cell transmittance and the cosh fit of the polarized cell to unpolarized cell ratio over neutron wavelength typically give 1% errors in the determination of  $\Theta$  and the product of  $P_{He}$  and  $\Theta$  respectively.

Further in this particular measurement, the in-situ polarization of the  $^3\text{He}$  analyzer was not yet available [11, 14], therefore the  $^3\text{He}$  polarization was indeed a function of time. The time

dependence of the decay of the  $^3\text{He}$  polarization was determined by performing unpolarized neutron transmittance measurements of the direct neutron beam as a function on neutron wavelength at 12 hour intervals during the measurement (i.e. between each pair of  $I^{00}$ ,  $I^{10}$  and  $I^{01}$ ,  $I^{11}$  scans). During these calibration measurements the sample and incident beam polarizer are momentarily translated out of the neutron beam, and a transmittance scan for  $\lambda=5\text{ \AA}$ - $10\text{ \AA}$  in five steps of the  $^3\text{He}$  cell is recorded. An attenuator can be placed in the beam to prevent detector saturation if needed. The resulting transmittances are then fit to eq. (15) fixing the values of  $T_0$  and  $\Theta$  to those obtained from unpolarized cell measurements to give  $P_{He}$  at the different times. These  $P_{He}$  values are then fit to

$$P_{He}(t) = P_{He}^0 \exp(-t/t_1) \quad (16)$$

to give us  $t_1$  which is the  $^3\text{He}$  polarization decay time constant and where  $P_{He}^0$  is the initial  $^3\text{He}$  polarization at time  $t = 0$ . For this experiment a  $t_1$  of  $156(\pm 4)$  hours was obtained which was then used to calculate  $T$  and  $A$  of the  $^3\text{He}$  cell at anytime for the  $\lambda=10\text{ \AA}$  neutron wavelength that we used for the reflectometry experiment. The initial and final analyzer efficiency were  $A^i = 99.9988(1)\%$  or  $p_2^i = 6.1(6) \times 10^{-5}$  and  $A^f = 99.971(1)\%$  or  $p_2^f = 1.5(1) \times 10^{-3}$  and the initial and final transmittance where  $T = 6.4(1)\%$  and  $T = 1.8(1)\%$  respectively. The relative transmissions are only important for comparing relative intensities taken at different times for the case of a time-changing  $P_{He}$ . Since the maximum time difference between  $\alpha_i$  data used in the intensity corrections was approximately 12 hours, or less than  $1/10$  of a decay time constant, the effects of the correction is not as extreme as total change in transmittance over the whole experiment.  $A$  was very high and the corresponding  $T$  low in this measurement due to the  $^3\text{He}$  cell which is optimized to also have a good value of  $A$  at the minimum MARIA wavelength of  $4.5\text{ \AA}$ . Additional corrections for the physical path length of the neutron through the  $^3\text{He}$  cell [12] were small for data of interest in our case and not considered in the analysis, however an expanded discussion of this effect is also given below. Further the very high analyzing efficiency at  $10\text{ \AA}$  also allows us to determine the remaining  $P$  and  $F$  parameters accurately [13].

Once the  $^3\text{He}$  polarization is determined to an appropriate accuracy, the incoming neutron polarization  $P$  and incident beam flipper efficiency  $F$  are determined using the polarized  $^3\text{He}$  cell by performing two flipping ratio measurements of the polarized neutron beam. The flipping ratios are then related to the total neutron polarization  $\mathcal{P}$  in the beam by

$$\mathcal{P} = \frac{\mathcal{F} - 1}{\mathcal{F} + 1} \quad (17)$$

where two flipping ratios are determined by using the  $^3\text{He}$  AFP flipper to reverse the analyzer's polarization direction while measuring the transmitted neutron beam intensity for both  $^3\text{He}$  polarization states with the incident beam flipper on and off. One obtains  $\mathcal{F}^{\text{on}}$  and  $\mathcal{F}^{\text{off}}$  which are the ratios of the intensities in the bright transmission state to the dark state with the incident beam flipper on or off respectively. This measurement then gives the total neutron polarization, or the product of all the neutron polarization efficiencies. For MARIA our incident polarization is a fixed double bounce reflection supper mirror polarizer which provides a stable neutron polarization parallel to the applied magnetic field on it. This polarization can then be flipped anti-parallel to the field with the incident beam RF gradient neutron flipper [6] which has inefficiency  $f_1$ . When the incident beam flipper is off it has no effect on the polarization efficiency so we measure  $PA$ , the product of the polarizer and analyzer polarizations. Conversely, when the incident beam flipper is active, or on, the small inefficiency of this flipper will lower the resulting flipping ratio and we obtain the product  $PAF$ . Therefore the ratio of  $\mathcal{P}^{\text{on}}/\mathcal{P}^{\text{off}}$  gives the flipper efficiency  $F$  which is related to the flipper inefficiency by  $f_1 = (1 - F)/2$ .

Now, from the above eq. (14) we can solve for  $A$  to determine  $p_2$  and then determine the value of  $P$  (i.e.  $p_1$ ) independently. If the measurement is done using multiple neutron wavelengths we



can perform this two flipping ratio analysis at the desired wavelengths used for a measurement because on MARIA, or any instrument using a super mirror or crystal polarizer, the incoming neutron polarization and flipper efficiency can be a function of neutron wavelength and beam apertures or focusing. Consequently this method using a  $^3\text{He}$  spin filter is particularly attractive for sensitive polarized neutron measurements because it is done for the specific instrument configuration of the actual sample measurement. On MARIA this is generally done by first aligning the sample, configuring the measurement, and then simply translating the sample out of the beam to quantify the instruments polarization efficiencies for the exact instrument and sample environment configuration using the direct beam at the time of the experiment.

From these flipping ratio measurements, the incident beam polarization  $P$  was 98.56(1)% or  $p_1 = 7.2(1) \times 10^{-3}$  and the flipper efficiency  $F = 1 - 2f_1$  was 99.20(2)% or  $f_1 = 4.0(1) \times 10^{-3}$ . These given errors follow from the 1% error in the determination of the  $^3\text{He}$  cell parameters as discussed above and because the  $^3\text{He}$  cell was “opaque” for the 10 Å neutron wavelength in this experiment providing an analyzing inefficiency an order of magnitude lower than the flipper and polarizer inefficiencies allowing for accurate determination of these parameters [13].

The cells used for analysis on MARIA are from GE180 tubing reblown into glass cylinders of suitable dimensions and thus have slightly rounded faces and corners. However the cells we used have a relatively low curvature in the neutron faces, and the area on the edges of the cylinder are masked with a neutron absorber. W C Chen et. al. [12] showed that the path length correction  $l/l_0$  for such a cell is;

$$\frac{l}{l_0} \simeq 1 + \left[ \frac{1}{2} \left( 1 - \frac{l_0}{2R} \right) - \frac{D_{sc}^2}{Rl_0} \right] \tan^2(2\theta) - \frac{D_{cd}^2}{Rl_0} \frac{A_s}{2\pi(D_{sc} + D_{cd} + l_0)^2} \quad (18)$$

where  $l_0$  is the assumed neutron path length through the middle of the cell,  $R$  is the radius of curvature of the ends of the cell,  $D_{sc}$  and  $D_{cd}$  are the sample to cell and cell to detector distances respectively,  $2\theta$  is the scattering angle, and  $A_s$  is the cross sectional area of the sample where a SANS transmission scattering geometry is assumed (i.e sample perpendicular to the incident beam). The cell used on MARIA for this experiment has  $l_0 \simeq 8\text{ cm}$ ,  $R > 100\text{ cm}$ ,  $2\theta_{max} = 0.080\text{ rad}$ ,  $D_{sc} = 60\text{ cm}$  and  $D_{cd} = 132\text{ cm}$ . The sample was  $2\text{ cm} \times 2\text{ cm}$ , where for reflectometry it is placed at a small angle resulting in an over estimation of this sample size correction term for our geometry, however this term is very small in our case. MARIA uses an elliptically focusing guide to increase the neutron intensity on the sample [1] and the calibration measurement of  $A$  and  $T$  to determine the  $P_{He}$  and  $\Theta = l_0[\text{He}]$  uses the same vertical focusing and is actually a cell-volume average so no further correction of  $A$  or  $T$  should be needed for the specular line which always passes through the center of the cell. Returning to the off specular scattering, using the path length correction from eq.(18) and eqs. (14), (15) for our cell, which has a path length  $^3\text{He}$  density product of 9.27 bar cm with maximum and minimum polarization of 71.5% to 52.6% in this experiment, we can estimate the effects of the path length correction on our data. The maximum error in  $A$  using these values is below  $1 \times 10^{-4}$  and can be ignored. For  $T$  (eq. (15) used to correct the neutron transmittances) the resulting maximum correction could be up to 9%, however this is at the maximum  $\alpha_f$  of  $\pm 80\text{ mRad}$  from the specular scattering which passes through the center of the cell. The data of interest in this experiment had an  $|\alpha_i - \alpha_f| < 25\text{ mRad}$  so the possible path length dependent correction would be  $< 1\%$  for  $T$  in this range. Since as was described in section 4 the statistical error bars of our intensities were around 3% for the spin-flip scattering we have ignored the path length correction in our analysis. For some geometries and cell opacities ( $\Theta$ ) the path length corrections can become important and should be calculated and included when normalizing the intensities to the  $^3\text{He}$  transmittance and correcting for the analyzing power. This can be done for each  $\alpha_f$  line similar to the way the time dependence was corrected for the individual  $\alpha_i$  lines.



## References

- [1] Heinz Maier-Leibnitz Zentrum, Forschungszentrum Jülich, Jülich Centre for Neutron Science 2015 *J of large-scale research facilities* **1** A8. [DOI: 10.17815/jlsf-1-29]
- [2] Wildes A 1999 *Review of Scientific Instruments* **70** (11):4241-4245. [DOI: 10.1063/1.1150060]
- [3] Wildes A R 2006 *Scientific Reviews: Neutron Polarization Analysis Corrections Made Easy, Neutron News* **17:2** 17-25 [DOI: 10.1080/10448630600668738]
- [4] Abragam A 1961 *The Principles of Nuclear Magnetism* Oxford University Press, Oxford, England
- [5] Jones G L, Dias F, Collett B, Chen W C, Gentile T R, Piccoli P M B, Miller M E, Schultz A J, Yan H, Tong X, Snow W M, Lee W T, Hoffmann C, Thomison J 2006 *Physica B: Condensed Matter* **385?386** 1131-1133 [DOI:10.1016/j.physb.2006.05.390]
- [6] Babcock E, Petoukhov A, Chastagnier J, Jullien D, Lelièvre-Berna E, Andersen K H, Georgii R, Masalovich S, Boag S, Frost C D, Parnell S R 2007 *Physica B* **397** 172-175. [DOI: 10.1016/j.physb.2007.02.093]
- [7] McKetterick T J, Boag S, Stewart J R, Frost C D, Skoda W M A, Parnell S R, Babcock E 2011 *Physica B* **406** 2436-2438. [DOI: 10.1016/j.physb.2010.11.088]
- [8] Ehlers G, Stewart J R, Deen P P, Andersen K H 2015 *European Physical J of Conf* **83** 03004. [DOI: 10.1051/epjconf/20158303004]
- [9] Andersen K H, Cubitt R, Humblot H, Jullien D, Petoukhov A, Tasset F, Schanzer C, Shah V R, Wildes A R, 2006 *Physica B: Condensed Matter* **385-386** 1134-1137. [DOI: 10.1016/j.physb.2006.05.391]
- [10] Salhi Z, Babcock E, Pistel P, Ioffe A 2014 *J of Physics Conference Series* **528(1)** 012015 [DOI: 10.1088/1742-6596/528/1/012015]
- [11] Babcock E, Salhi Z, Theisselmann T, Starostin D, Schmeissner J, Feoktystov A, Mattauch S, Pistel P, Radulescu A, Ioffe A 2016 *J of Physics Conference Series* **711** 012008 [DOI: 10.1088/1742-6596/711/1/012008]
- [12] Chen W C, Erwin R, Watson S M 2013 *Physics Procedia* **42** 163-170. [DOI: 10.1016/j.phpro.2013.03.191]
- [13] Klauser C, Chastagnier J, Jullien D, Petoukhov A, Soldner T 2012 *J of Phys: Conf Series* **340** 012011 [DOI: 10.1088/1742-6596/340/1/012011]
- [14] Babcock E, Mattauch S, Ioffe A 2010 *Nuclear Instruments and Methods in Physics Research Section A Accelerators Spectrometers Detectors and Associated Equipment* **625** 43-46 [DOI: 10.1016/j.nima.2010.09.078]
- [15] Theis-Bröhl K, Westphalen A, Zabel H, Rcker U, McCord J, Höink V, Schmalhorst J, Reiss G, Weis T, Engel D, Ehresmann A, Toperverg B P 2008 *New Journal of Physics* **10** 093021 [DOI:10.1088/1367-2630/10/9/093021]
- [16] Zabel H, Theis-Bröhl K, Wolff M, Toperverg B P 2008 *IEEE Transactions on Magnetics* **44** no. 7, 1928-1934 [DOI:10.1109/TMAG.2008.924538]
- [17] Toperverg B P 2015 *Physics of Metals and Metallography* **116** 1337-1375. [DOI: 10.1134/S0031918X15130025]
- [18] Durniak C, Ganeva M, Pospelov G, Van Herck W, Wuttke J 2015, **BornAgain** Software for simulating and fitting X-ray and neutron small-angle scattering at grazing incidence <http://www.bornagainproject.org>
- [19] Babcock E, Salhi Z, A Ioffe 2013 *J of the Physical Society of Japan* **82** (supp. A) SA030-10
- [20] Williams
- [21] Chupp T E, Coulter K P, Kandes M, Sharma M, Smith T B, Jones G, Chen W C, Gentile T R, Rich D R, Lauss B, Gericke M T, Gillis R C, Page S A, Bowman J D, Penttila S I, Wilburn W S, Dabaghyan M, Hersman F W, Mason M 2007 *Nuclear Instruments and Methods in Physics Research Section A: Accelerators, Spectrometers, Detectors and Associated Equipment* **574** 500-509. [DOI: 10.1016/j.nima.2007.02.091]
- [22] Rich D R, Bowman J D, Crawford B E, Delheij P P J, Espy M A, Haseyama T, Jones G, Keith C D, Knudson J, Leuschner M B, Masaike A, Masuda Y, Matsuda Y,6, Penttila S I, Pomeroy V R, Smith D A, Snow W M, Szymanski J J, Stephenson S L, Thompson A K, Yuan V 2002 *Nuclear Instruments and Methods in Physics Research A* **481** 431-453. [DOI: 10.1016/S0168-9002(01)01331-6]
- [23] Chen W C, Gentile T R, Fu C B, Watson S, Jones G L, McIver G L, Rich G L 2011 *J of Physics: Conference Series* **294** 012003 [DOI:10.1088/1742-6596/294/1/012003]
- [24] Petoukhov A K, Andersen K H, Jullien D, Babcock E, Chastagnier J, Chung R, Humblot H, Lelivre-Berna E, Tasset F, Radu F, Wolff M, Zabel H 2006 *Physica B: Condensed Matter* **385?386** Part 2 1146-1148 doi:10.1016/j.physb.2006.05.394
- [25] Andersen K H, Cubitt R, Humblot H, Jullien D, Petoukhov A, Tasset F, Schanzer C, Shah V R, Wildes A R 2006 *Physica B: Condensed Matter* **385-386** Part 2 1134-1137 [DOI: 10.1016/j.physb.2006.05.391]